Advanced Steel Construction – Vol. 18 No. 2 (2022) 604–616
DOI:10.18057/IJASC.2022.18.2.9

SEISMIC PERFORMANCE OF SINGLE-LAYER SPHERICAL RETICULATED SHELLS CONSIDERING JOINT STIFFNESS AND BEARING CAPACITY

Hui-Huan Ma [1], Yue-Yang Ma [2, *], Feng Fan [3] and Ying-Nan Zhang [2]

[1] *School of Civil Engineering, Sun Yat-sen University & Southern Marine Science and Engineering Guangdong Laboratory, Zhuhai, Guangdong, P. R. China*
[2] *Shanghai Construction No.4 (Group) Co., LTD., Shanghai, P. R. China.*
[3] *Harbin Institute of Technology, Harbin, PR China*
** (Corresponding author: E-mail: mayy_scc4@163.com)*

ABSTRACT

Fabricated joints are gradually applied in architectural structures because of their advantages of good economy, high installation quality and efficiency. However, the mechanical properties of this kind of joint are semi-rigid differing from traditional rigid and hinged joints. Therefore, the performance of the structures with such joints is not clear, which greatly limits the wide application of fabricated joints. This paper presents the investigation on the seismic performance of the semi-rigid single-layer reticulated shell structure (SRSS) under earthquake load by numerical simulation and theoretical analysis. A finite element model (FEM) of the semi-rigid reticulated shell was established. The influence of joint stiffness on the seismic performance of semi-rigid SRSS was obtained by taking both initial defects and material damage accumulation into account. The two design parameters, limit stiffness ratio and limit yield moment of the joints, were proposed for the semi-rigid reticulated shells. The influence of the roof span, roof weight and member section on the two design parameters was obtained and the calculation formula was established. The seismic force coefficient for the semi-rigid SRSS was obtained, which can provide support for the seismic design of semi-rigid SRSS.

ARTICLE HISTORY

Received: 8 February 2022
Revised: 16 May 2022
Accepted: 16 May 2022

KEYWORDS

Semi-rigid joint;
Joint stiffness;
Single-layer reticulated shell structure;
Seismic performance;
Seismic design

1. Introduction

Single-layer reticulated shell structure (SRSS) is a typical large-span space structure [1-2], which has the characteristics of good economy, stability and seismic performance. These kinds of structures are commonly large-scale public buildings and are used as temporary earthquake shelters. However, the past earthquake damage showed that this kind of structure also could be damaged or even collapsed in varying degrees (Fig. 1). The joints are the key components of the transmission force between members. The performance of joints has a significant impact on the seismic response of the structure.

Fabricated joints are gradually applied in many kinds of buildings because of their advantages of good economy, high installation quality and efficiency. However, the mechanical properties of this kind of joint are semi-rigid differing from traditional rigid and hinged joints. The performance of the structures with such joints is not clear which limits the application of the fabricated joints.

(a) Instability of member (b) Fracture of joint

Fig. 1 The past earthquake damage

Firstly, the research on the static performance of traditional joints was carried out. The moment-rotation curves (M-Φ curves) of bolted ball joints [3] and bowl joints [4] under axial force and bending moment were obtained. Afterward scholars developed new joints with stronger bearing capacity and higher stiffness, such as CP joints [5], AAP joints [6], steel dovetail joints [7], gear joints [8], bolt column joints [9], threaded-sleeve joints [10], etc.

The study on the hysteretic performance of space fabricated joints mainly focused on the frame structure [11-12]. However, related research on the joints of large span space structures is limited. Ma [13] conducted the numerical simulation of the hysteretic behavior of CP joints. The results presented that the joint energy-dissipating capacity was sensitive to the axial force. The tests for dynamic behavior of the gear joints were conducted in reference [14]. It proposed that the initial installation gap could lead to obvious pinch of the joint hysteretic curve.

With further research on the mechanical behavior of semi-rigid joints, researchers have gradually carried out the research on the static performance of semi-rigid reticulated shells. See [15], Fathelbab [16] and El Sheikh [17] investigated the static performance of the SRSS with bolt ball joints, and found that the effects of joint stiffness on overall structural bearing capacity cannot be neglected. Ma [18-19] established the FEM of reticulated shell considering joint stiffness, and the influence law of joint stiffness on the structural bearing capacity was obtained. The results of reference [20-21] pointed out that the stiffness and bearing capacity of semi-rigid socket joints and hollow ball-tube bolted joints can satisfy the requirements for SRSS with small and medium spans.

The above research verifies the feasibility of the application of semi-rigid joints in SRSS. The researchers then studied the seismic performance of semi-rigid SRSS. The dynamic behavior of semi-rigid SRSS was analyzed by Liao [22], which presented that the actual behavior and work performance of the SRSS can be analyzed more accurately by considering semi-rigid connections. The influence law of the joint stiffness on the dynamic performance of the semi-rigid SRSS was studied [23]. References [24-25] showed that the joint axial

stiffness impacted greatly on the structural free vibration properties and the member internal force.

In this paper, based on the theoretical model of gear joint [8], the FEM of the semi-rigid SRSS was built. The influence of joint stiffness on the characteristic response of reticulated shells with different spans, rise span ratios, roof weight and member section size was discussed. The seismic design method of semi-rigid SRSS was proposed, where two joint design parameters, the limit stiffness ratio and the limit yield moment, were determined. Meanwhile, the seismic internal force coefficients of main ribs, inclined bars and ring bars of semi-rigid SRSS were obtained, which can provide support for seismic design of the semi-rigid SRSS.

2. The semi-rigid gear joints

The gear bolt is the key component of the gear joint, which is the combination of bolt and gear, giving the hinged joint enough rotation stiffness while keeping good assemblability. The members can be connected to joint at any angle by rotating around three axes (x, y and z), as shown in Fig. 2. In the factory, the middle plate is welded with the ball according to the design angle, meanwhile, the side plates, end plate and member are also welded. At the construction site, construction workers simply complete the assembly process by inserting the gear bolt into the reserved hole on the connecting plate and tightening the bolts.

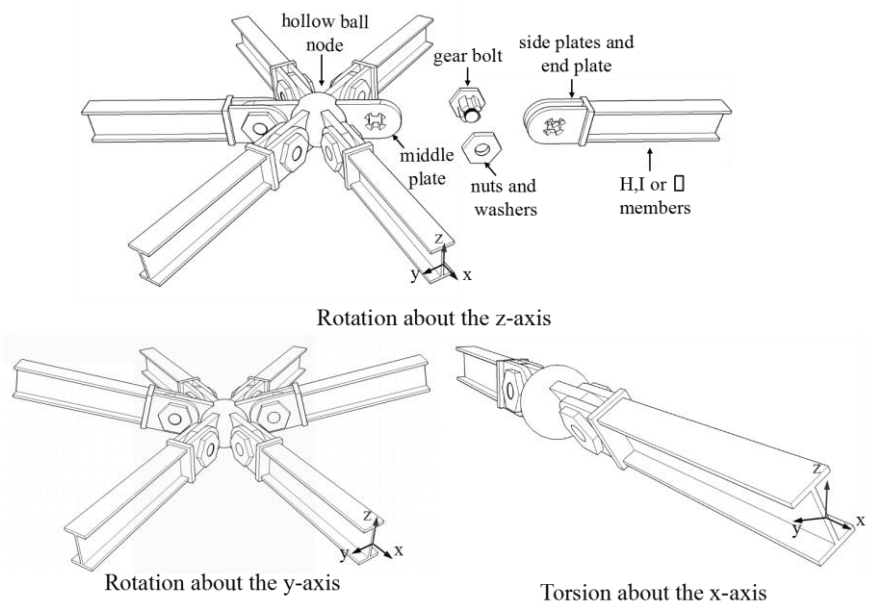

Fig. 2 Gear joint system

Several groups of tests for gear joints with different parameters were carried out in reference [8] (Fig.3), where the influence laws of gear bolt diameter (d), tooth number (n) and tooth height (t) on the mechanic behavior of gear joint were obtained. The joint was simplified into a spring model by the component method, as shown in Fig.4, then the theoretical calculation formulas of the joint initial stiffness ($S_{j,ini}$) and ultimate bending moment (M_u) and fitting formula of the M-Φ curves (formula (1)) were proposed, where n_s is the curve shape coefficient. For different dimensions of gear joints, the M-Φ curves can be fitted by adjusting the value of $S_{j,ini}$, M_u and n_s. The comparison between the test results and formula (1) is shown in Fig 5, as can be seen that the theoretical calculation has good accuracy.

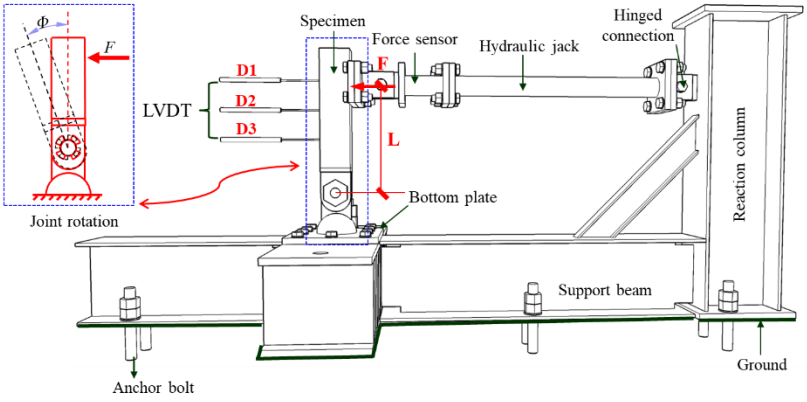

(a) Setting of the experimental device

(b) Before loading (c) After loading

Fig. 3 Test for gear joint[8]

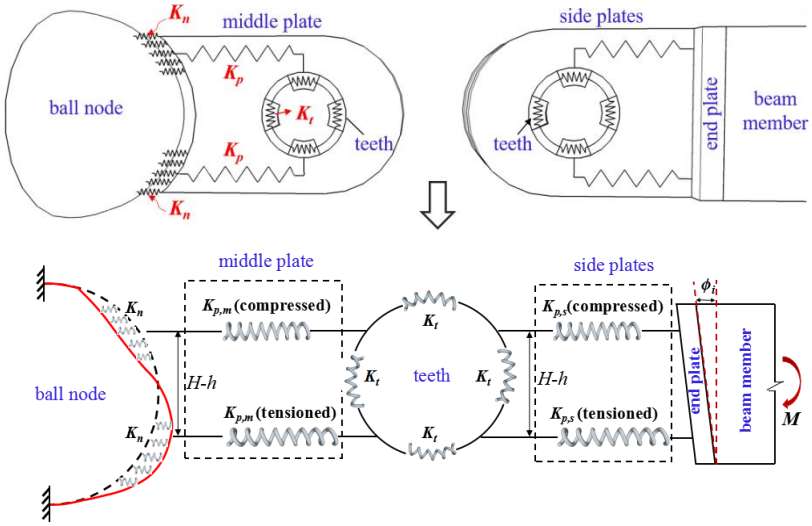

Fig. 4 Spring-stiffness model for the gear joint[8]

$$\Phi = \frac{M}{S_{j.ini}} \frac{1}{[1-(M/M_u)^{n_s}]^{1/n_s}} \tag{1}$$

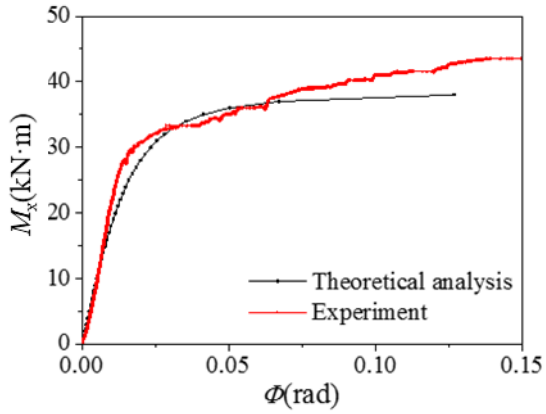

（a）T1-A (*d*=50mm, *n*=4, *t*/*d*=1/3)

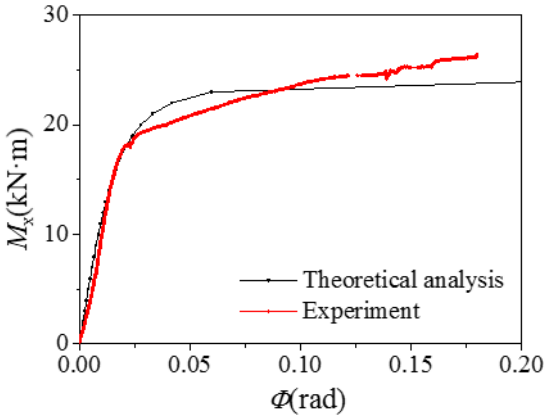

（b）T2-B (*d*=40mm, *n*=4, *t*/*d*=1/3)

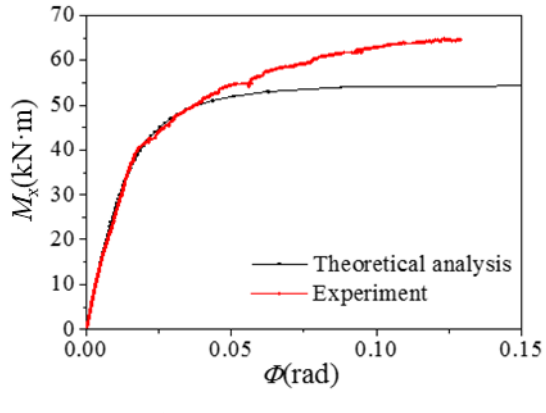

（c）T2-C (*d*=60mm, *n*=4, *t*/*d*=1/3)

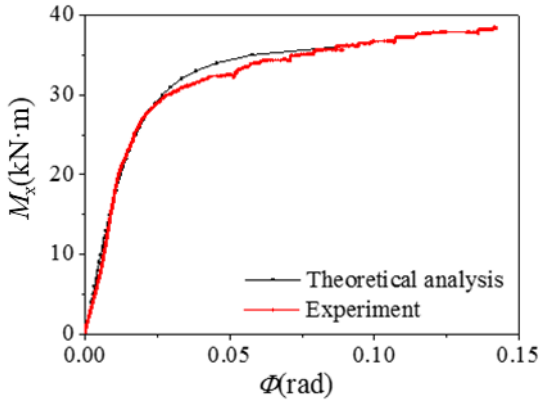

（d）T3-B (*d*=50mm, *n*=4, *t*/*d*=1/4)

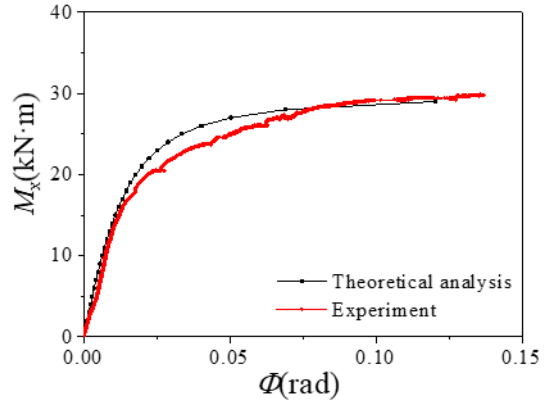

（e）T3-C (*d*=50mm, *n*=4, *t*/*d*=1/6)

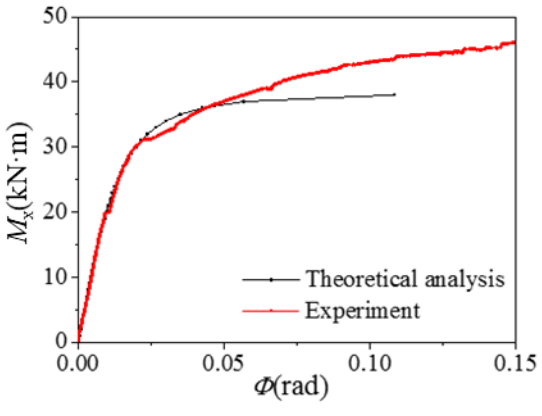

（f）T4-B (*d*=50mm, *n*=6, *t*/*d*=1/3)

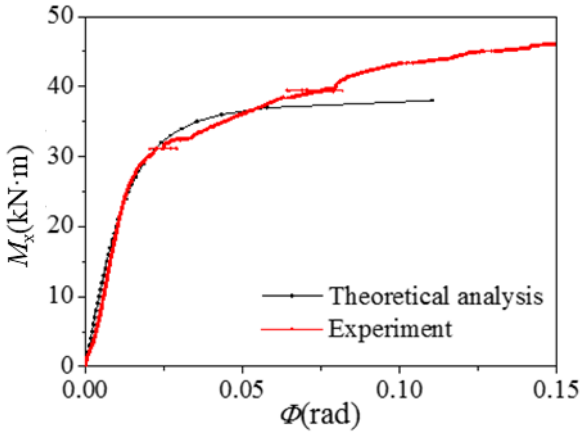

（g）T4-C (d=50mm, n=8, t/d=1/3)

Fig. 5 Comparison between tests and theoretical-analysis results of gear joints about x-axis[8]

3. The finite element model of SRSS with gear joint

The FEM of the semi-rigid SRSS was established by ABAQUS as shown in Fig. 6, where the joint area is set as rigid. The B31 elements and connector elements were adopted to simulate the members and joints. The values of joint stiffness and bearing capacity were obtained from the performance analysis of gear joints [8]. Rectangular section member was used in this model and the local coordinate system was established for each member. Moreover, the parameters of three axes (x, y, z-axis) of the connector should be set respectively. According to the characteristics of gear joints, the ratio of triaxial stiffness is 1: 0.28: 0.1.

The parameters of the FEM are listed in Table 1, where K_m is the linear stiffness of the members, which can be calculated by the formula (2), where E, I and l_m are young's modulus, section moment of inertia and calculation length of the member, respectively.

$$K_m = \frac{EI}{l_m} \tag{2}$$

$K_{m,min}$ is the minimum value of the linear stiffness of the members which meets the requirements of static design. The boundary condition is three-dimensional fixed hinge bearing. The stiffness ratio (α_k) is the ratio of the joint stiffness to the linear stiffness of the member. Joints and members are the key parts of the SRSS. Therefore, in this paper, the seismic design method of SRSS was proposed, which includes three aspects: joint stiffness design method, joint bearing capacity design method and member design method. The key design parameters are the limit stiffness ratio, the limit yield moment of the joint and the seismic internal force coefficient, accordingly.

The numbering rules of numerical examples are as follows: S4007060, for example, S represents SRSS, 40 represents L of 40m, 07 represents f/L of 1/3, and 120 represents w of 120kg/m^2. In addition, the effects of three-dimensional earthquake, material damage accumulation and initial imperfection are considered, the value of which is 1/300 of the span.

Table 1
Parameters of FEM of reticulated shells

Parameters	Value
Span (L)	40m-90m
Rise span ratio (f/L)	1/3-1/7
Roof weight (w)	60, 120, 180 (kg/m^2)
Linear stiffness of members	(1.0-10) $K_{m,min}$
Stiffness coefficient	α_k = 0.05-150
Joint bearing capacity	∞
Ground motion	Taft, El-Centro, Parkfield, etc.
Boundary condition	Hinge

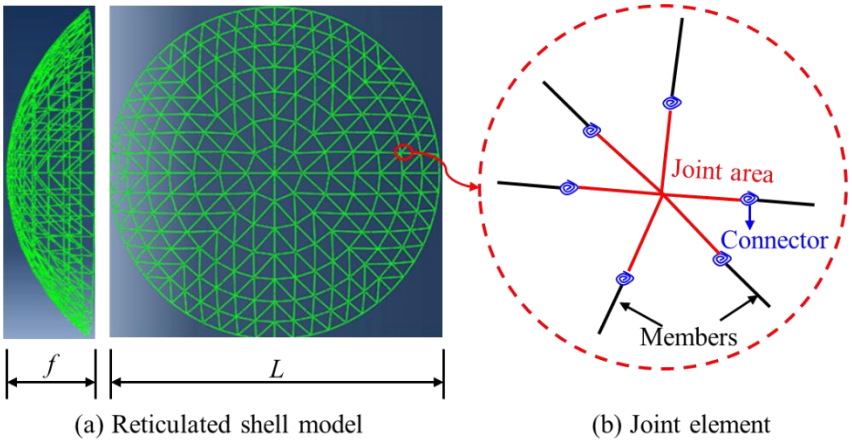

Fig. 6 Setting of joint connection

4. Analysis and calculation method of the seismic internal force coefficient

The seismic internal force coefficient ξ_e used in the design of lattice shell members can be calculated as follow:

$$\xi_e = \left| \left(\sigma_E + \sigma_{SV}\right)^{max} \Big/ \sigma_{SV}^{max} \right| \tag{3}$$

Where $\left(\sigma_E + \sigma_{SV}\right)^{max}$ is the maximum internal force of the member under the combination of earthquake and gravity load, σ_{SV}^{max} is the maximum static internal force of the member under gravity load.

If the ξ_e of each member is calculated, it will lose the practical significance of simple design for the SRSS with a large number of members. Therefore,

according to the classification of members, the members were divided into main members, circle members and diagonal members. The maximum stress values of three types of members were respectively counted, and the member with maximum stress was chosen as the control member.

The ground motions in Table 2 were selected for analysis and their amplitudes were modulated according to the acceleration peak value of frequent earthquakes of degree 8. Fig. 7 to Fig.9 show the influence of different span, rise span ratios and roof weight of reticulated shells on the maximum member stress under seismic action. It can be seen that the variation law of maximum member stress with stiffness ratio is similar under different parameters. The maximum stress of main members and diagonal member decreases with the increase of stiffness ratio, but the decrease range is very small. However, the stiffness ratio has no obvious effect on the circle member stress.

Table 2
Parameters of ground motion

ID	Name of ground motion	Magnitude	Time
1	Loma Prieta	6.93	1989
2	Parkfield	6.19	1966
3	Imperial Valley	6.53	1979
4	Victoria, Mexico	6.33	1980
5	Coalinga	6.36	1983
6	Morgan Hill	6.19	1984
7	N. Palm Springs	6.06	1986
8	Superstition Hills	6.54	1987
9	Cape Mendocino	7.01	1992
10	Landers	7.28	1992
11	Northridge	6.69	1994
12	Kobe, Japan	6.90	1995
13	Kocaeli, Turkey	7.51	1999
14	Hector Mine	7.13	1999
15	Taft	7.52	1952

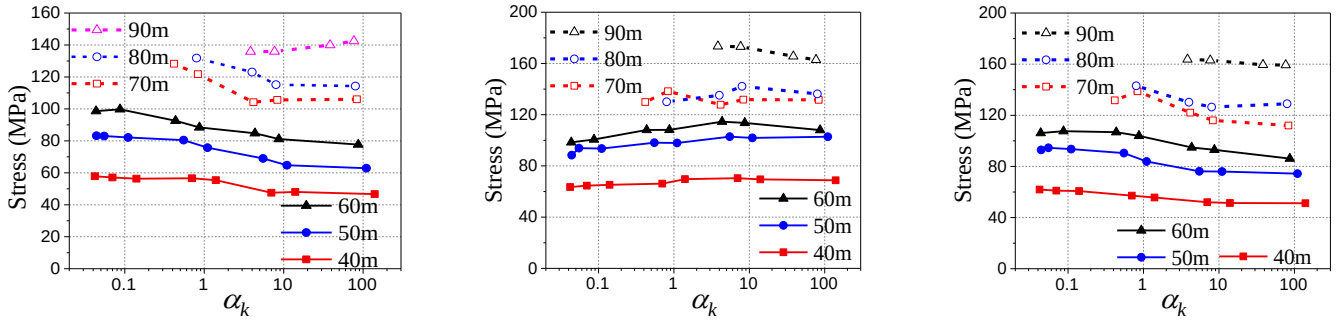

(a) Main members (b) Circle members (c) Diagonal members

Fig. 7 Influence of reticulated shell span on maximum member stress

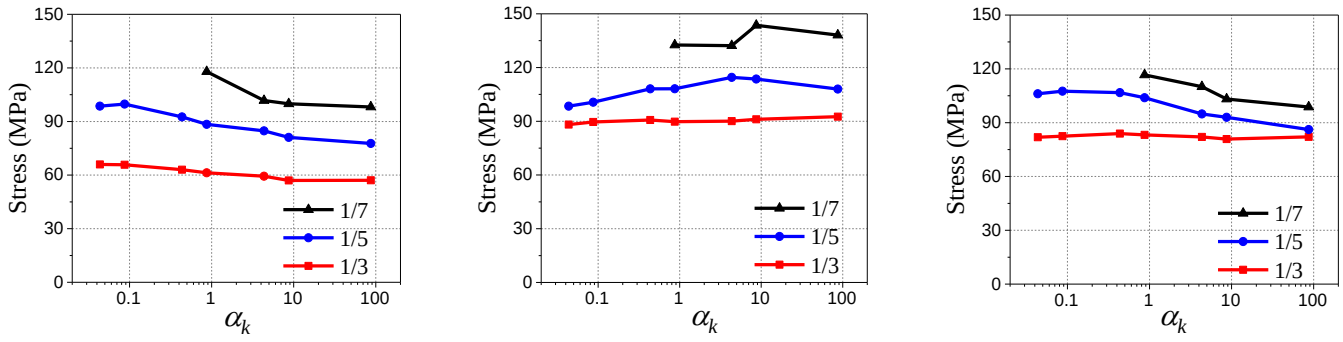

(a) Main members (b) Circle members (c) Diagonal members

Fig. 8 Influence of rise-span ratio on maximum member stress

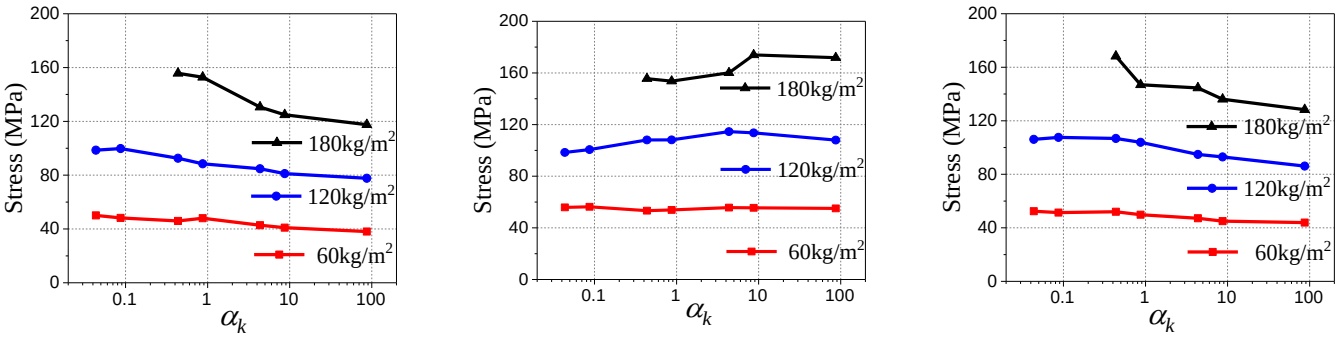

(a) Main members (b) Circle members (c) Diagonal members

Fig. 9 Influence of roof weight on maximum member stress

The ξ_e of all kinds of member are showed in Fig. 10 to Fig. 12. It shows that the value of coefficient ξ_e of main members and diagonal members decreases with the increase of stiffness ratio, which is similar to the change of member stress, and with the increase of the span and roof weight, reduction of rise span ratio, the value of coefficient ξ_e of the main members increases gradually. However, different from the stress variation of members, there is no obvious law between the value of coefficient ξ_e of circle member and diagonal member and the span, rise span ratio and roof weight of reticulated shells. On the contrary, some values of coefficient ξ_e of latticed shells with larger span, larger roof weight and smaller rise span ratio are smaller, because the stress of this kind of reticulated shell is significant under the gravity load, on condition of which the increase of numerator is not as large as that of the denominator in the calculation of ξ_e, resulting in the decrease of ξ_e.

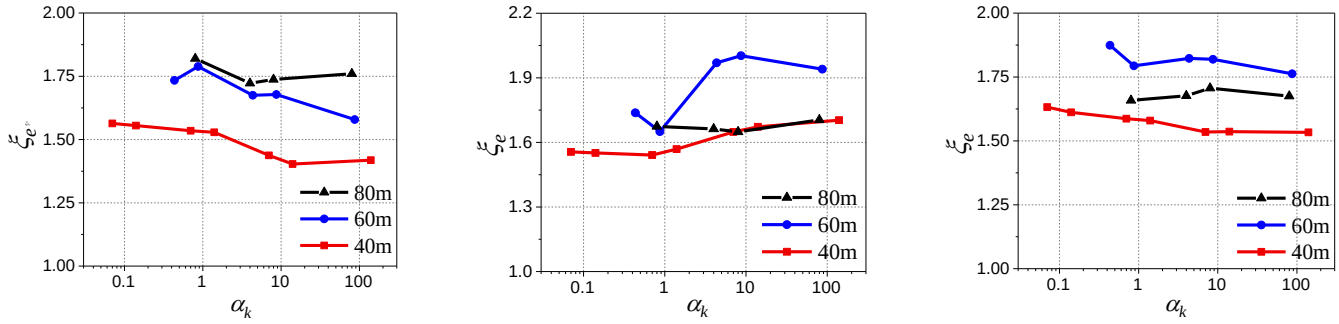

(a) Main members (b) Circle members (c) Diagonal members

Fig. 10 Influence of L on earthquake action coefficient

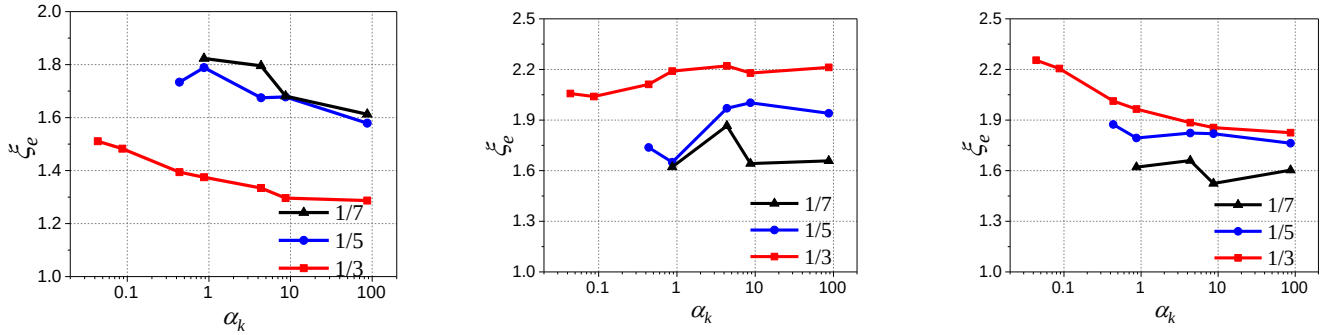

(a) Main members (b) Circle members (c) Diagonal members

Fig. 11 Influence of f/L on earthquake action coefficient

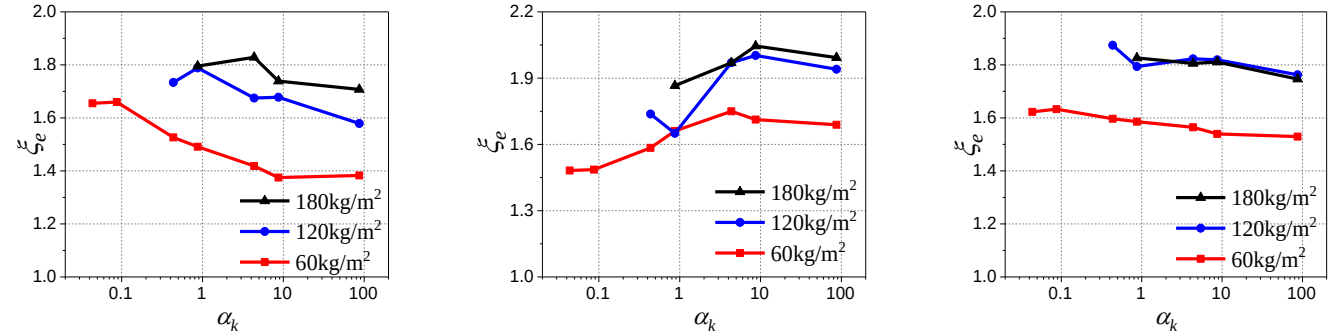

(a) Main members (b) Circle members (c) Diagonal members

Fig. 12 Influence of w on earthquake action coefficient

In order to facilitate engineering application, the values of coefficient ξ_e of various members in semi-rigid SRSS under different parameters are listed in Table 3.

Table 3
Earthquake action coefficient of semi-rigid SRSS

L (m)	f/L	w (kg/m^2)	Main members	Circle members	Diagonal members
40	1/5	120	1.56	1.70	1.63
	1/3	120	1.51	2.22	2.25
		60	1.66	1.75	1.63
60	1/5	120	1.79	2.00	1.87
		180	1.83	2.05	1.83
	1/7	120	1.82	1.87	1.66
80	1/5	120	1.82	1.70	1.71

5. Analysis and calculation method of limit stiffness ratio

Fig. 13 shows the displacement-time curves of S6005180 with different stiffness ratios. As can be seen from the figure: i) when the structure is only under the action of gravity load, the structural displacement with large stiffness is basically linear and increases gradually with the decrease of the stiffness ratio, but it still remains stable. Until the stiffness ratio is reduced to a certain extent (α_k=0.044 in this example), the displacement of structure will be great or divergence. ii) When the latticed shell is subjected to the seismic wave with peak ground acceleration (PGA) of 0.07g, the displacement of the structure changes little as the stiffness ratio changes in a certain range. Until the stiffness ratio is reduced to 0.087, the reticulated shell collapses. ii) When the PGA increases to 0.4g, the displacement of structure increases gradually with the decrease of the stiffness ratio and the equilibrium position of the joint vibration shifts, but the whole structure can maintain a stable vibration state. Until the stiffness ratio decreases to 4.4, the reticulated shell collapses. Moreover, the smaller the stiffness ratio is, the earlier the reticulated shell collapses

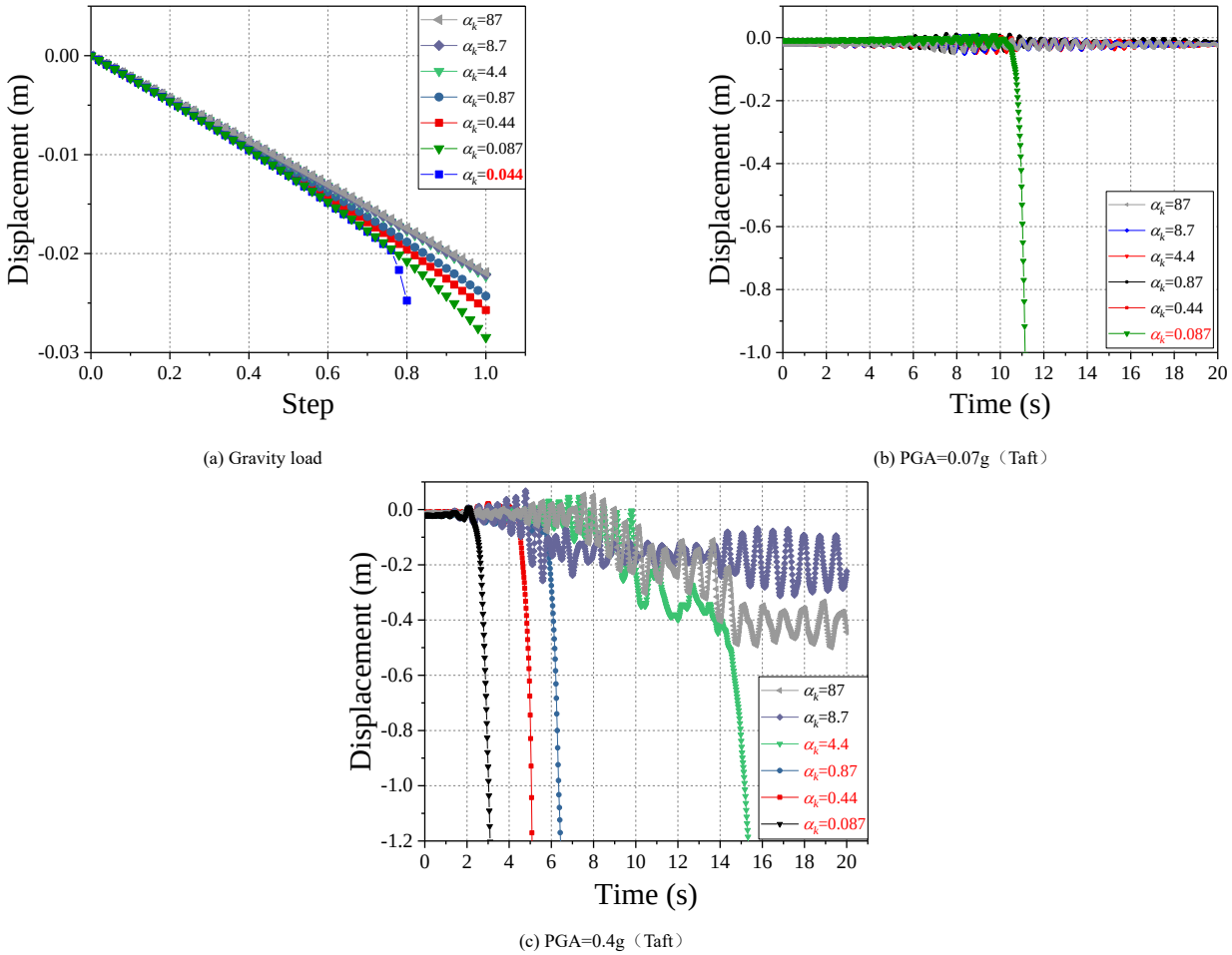

(a) Gravity load

(b) PGA=0.07g（Taft）

(c) PGA=0.4g（Taft）

Fig. 13 Displacement-time curves of S6005180 with different stiffness ratios

It can be seen that when other parameters remain unchanged, with the increase of load, the SRSS needs greater stiffness ratio to ensure stability. The minimum value of the stiffness ratio, which can keep the structure in stable status under a certain PGA, is defined as the limit stiffness ratio ($\alpha_{k,min}$). If $\alpha_k<\alpha_{k,min}$, the structure collapses. The value of the $\alpha_{k,min}$ also needs to consider the influence of the span (L), rise span ratio (f/L), roof weight (w) of reticulated shell, member section and ground motion. The influence of each parameter on the limit stiffness ratio is introduced below.

5.1. Influence of different structural parameters

Taking the SXX05120 (f/L=1/5, w=120 kg/m^2) as an example, the maximum displacement of the structure with varying span from 40m to 90m is plotted in Fig. 14. As shown in the figure: i) as increasing of the span, the maximum displacement response increases at the same stiffness ratio. ii) The stiffness ratio has little effect on the displacement of the reticulated shell with the same span, which has no obvious rule. iii) The abscissa of the leftmost point of each curve is the limit stiffness ratio of the reticulated shell. If the stiffness ratio is less than this value, the structural displacement does not converge or the whole structure will collapse. Meanwhile, as increasing of the span, the limit stiffness ratio increases gradually. iv) With the increase of the PGA, the maximum displacement response and the limit stiffness ratio increase. When the span of the reticulated shell and PGA are both small, the limit stiffness ratio of the SRSS is about 0.05, which is taken as the minimum value of the limit stiffness ratio in favor of safety.

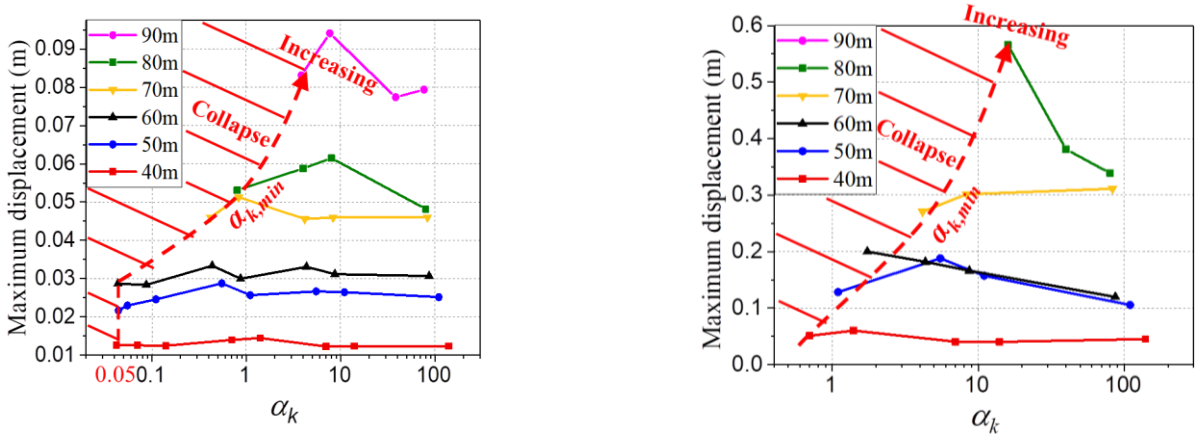

(a) PGA=0.07g (b) PGA=0.4g

Fig. 14 Influence of stiffness ratio on maximum displacement of structures with different spans

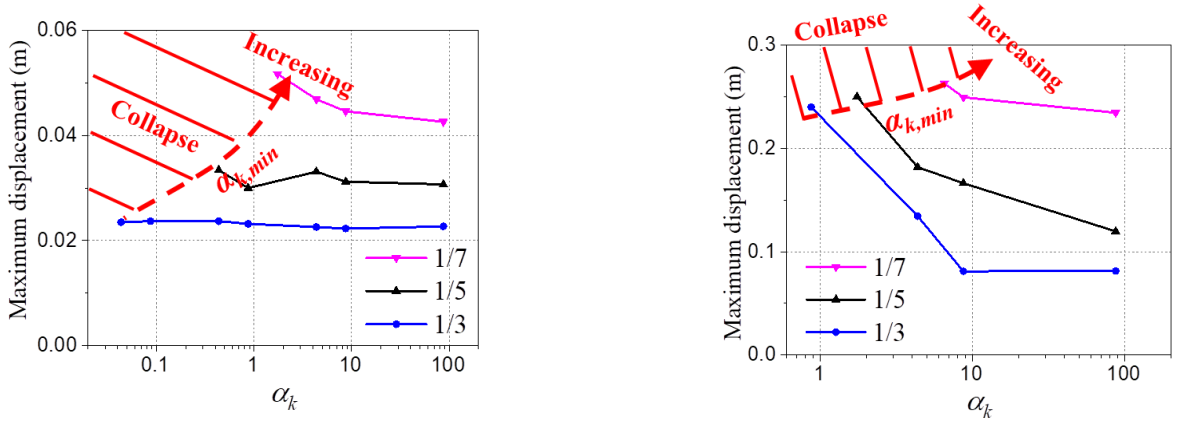

(a) PGA=0.07g (b) PGA=0.4g

Fig. 15 Influence of stiffness ratio on maximum displacement of structures with different *f*/*L*

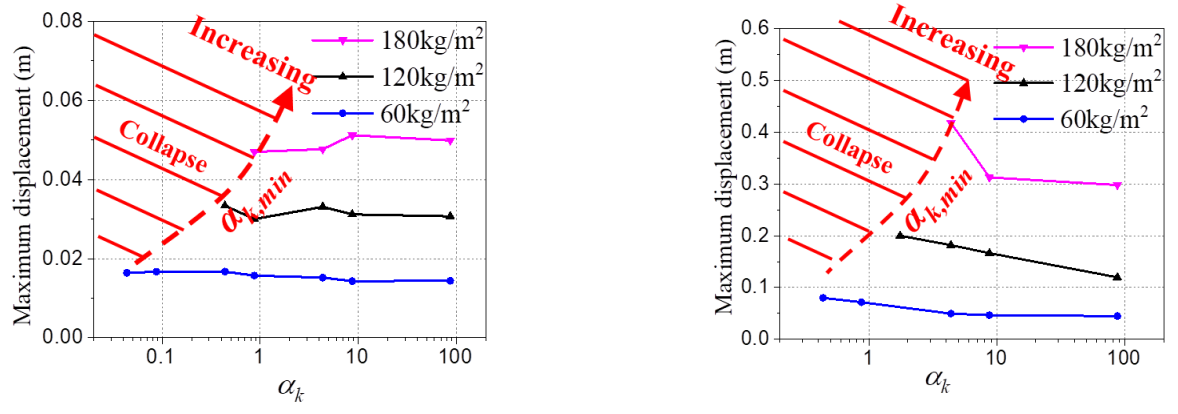

(a) PGA=0.07g (b) PGA=0.4g

Fig. 16 Influence of stiffness ratio on maximum displacement of shells with different *w*

Similarly, the maximum displacement of structures with different *f*/*L* and *w* is shown in Fig.15 and Fig.16. The figure presents that: i) with the decrease of *f*/*L* and the increase of *w*, the maximum displacement response of reticulated shell decreases with the same stiffness ratio. ii) the limit stiffness ratio becomes bigger gradually as the *f*/*L* decreases and *w* increases.

Generally speaking, the stiffness ratio has little effect on the maximum displacement response of SRSS, while the limit stiffness ratio is significantly affected by the *L*, *w*, *f*/*L* and seismic peak value. The bigger the span and roof weight, and the smaller the rise span ratio, the larger the stiffness ratio is needed to maintain the stability of the whole structure under the same seismic load.

The change of limit stiffness ratio of SRSS with different parameters is shown in Fig. 17. It can be seen that when one of the parameters becomes disadvantageous, the limit stiffness is more sensitive to the other two parameters. For example, when the rise span ratio of SRSS with the span of 60m decreases from 1/3 to 1/7, and the roof weight increases from 120 kg/m^2 to 240 kg/m^2, the limit stiffness ratio increases by 40 times and 3 times respectively. In the same case, for 80m reticulated shell, the limit stiffness ratio increases by 50 times and 3.33 times respectively.

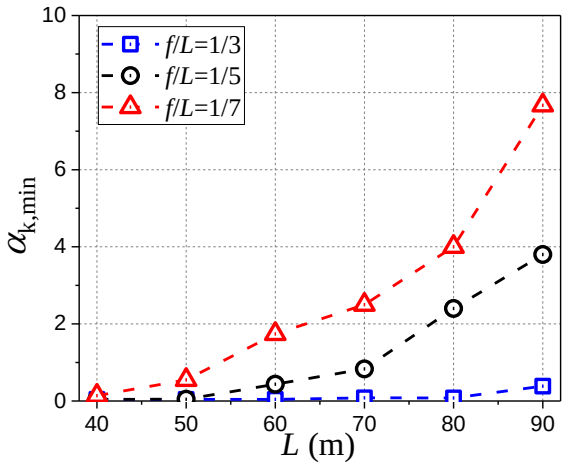

(a) Span-rise span ratio

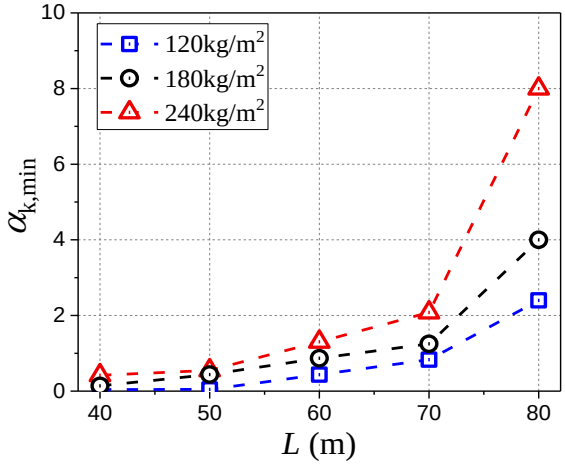

(b) Span - roof weight

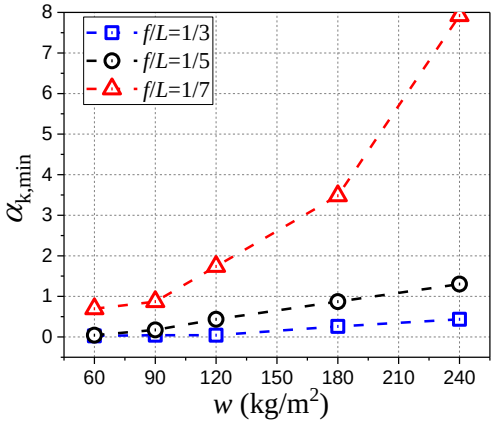

(c) Roof weight-rise span ratio

Fig. 17 Variation of limit stiffness ratio under different parameters of SRSS

5.2. Influence of member section

In this section, four member sections are used for analysis. The section numbers J1, J2, J3 and J4 are corresponding to $K_{m,min}$、$2K_{m,min}$、$4K_{m,min}$ and $10K_{m,min}$ respectively. The influence of member section on the limit stiffness ratio with different parameters is shown in Fig. 18, which shows that the limit stiffness ratio decreases with the increase of the section of the member. Meanwhile the larger the span , the bigger the roof weight and the smaller the rise span ratio, the greater the limit stiffness ratio is affected by the section of the member. Taking the SXX05120 (f/L=1/5, w=120 kg/m^2) as an example, when the member section of reticulated shell with the span of 80m is reduced from J4 to J1, the stiffness ratio needs to be increased by 123.5 times to maintain the stability of whole structure. However, the stiffness ratio of the shells with the span of 40m only needs to be increased by 13.2 times to meet the requirements. It also indicates that increasing the member section is more effective than increasing the joint stiffness for this kind of latticed shell. The member section reduction factor r_b was proposed to consider the impact of member section, and the value of r_b is calculated by formula (4), where β is the ratio of liner stiffness of the adopted member section to $K_{m,min}$.

$$r_b = 1.25\beta^2 - 0.25 \tag{4}$$

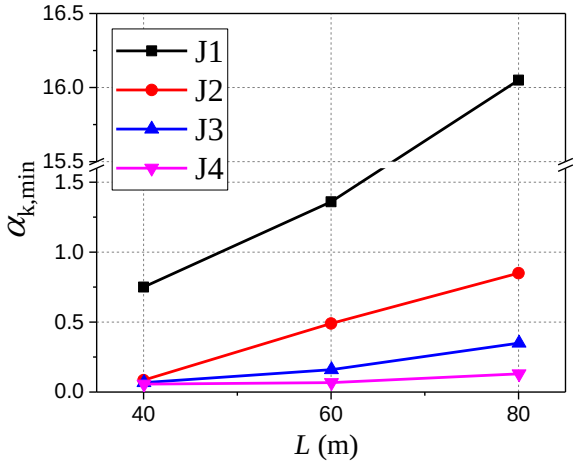

(a) Different span

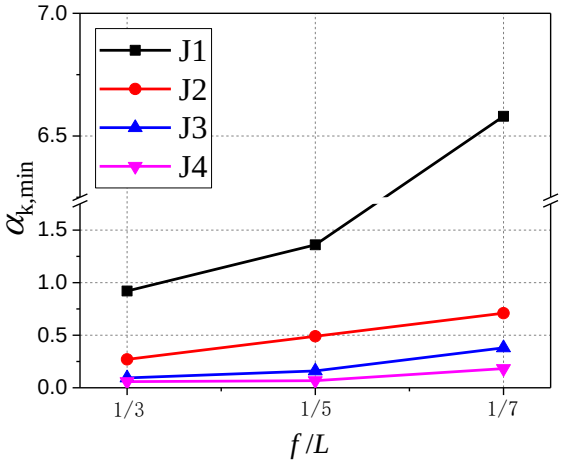

(b) Different rise span ratio

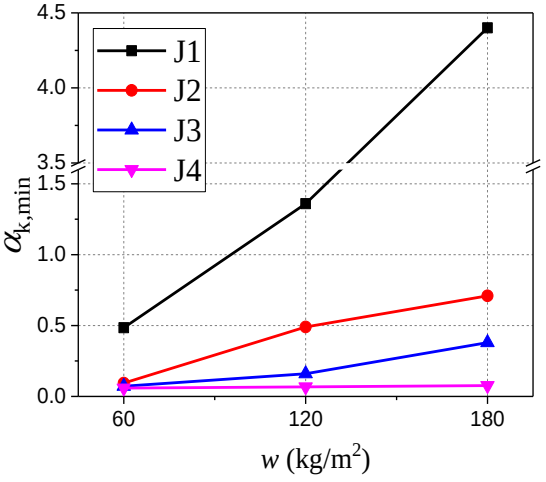

(c) Different roof weight

Fig. 18 Effect of member section on limit stiffness ratio of SRSS

5.3. Influence of ground motion

Fifteen different ground motions (Table 2) are selected to analyze the S6005120. The influence of ground motion on the limit stiffness ratio is presented in Fig. 19.The ground motion has a certain influence on the limit stiffness ratio, but the influence is less significant than that of the member section. The ground motion correction coefficient r_e is used to correct the influence, and its value can be calculated by the formula below:

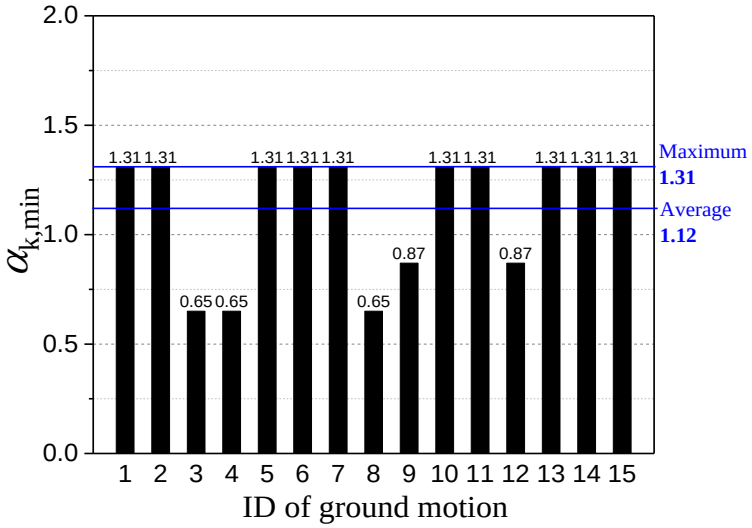

Fig. 19 Effect of ground motion on limit stiffness ratio of SRSS

$$r_e = \frac{\mathrm{Max}\left(\alpha_{k,min}\right)}{\mathrm{Ave}\left(\alpha_{k,min}\right)} \tag{5}$$

Max($\alpha_{k,min}$)-the maximum value of limit stiffness ratio of all ground motions
Ave($\alpha_{k,min}$)-the average value of limit stiffness ratio of all ground motions

5.4. Calculation formula of limit stiffness ratio

According to the relationship between the limit stiffness ratio and the parameters of the SRSS (Fig. 20), the power function (formula (6)) is used to calculate the limit stiffness ratio.

$$\alpha_{k,min} = \frac{L_\Delta}{S_w \mu_{fl}} \frac{1}{\left[1-\left(L_\Delta / L_{u,\Delta}\right)^{n_s}\right]^{1/n_s}} \tag{6}$$

where the value of horizontal coordinate L_Δ and the maximum value of horizontal coordinate $L_{u,\Delta}$ are mainly controlled by the span of the lattice shell and are calculated by formula (7) and formula (8).

$$L_\Delta = L - L_i \quad 30\mathrm{m} \le L \le 100\mathrm{m} \tag{7}$$

$$\begin{aligned} &\text{PGA=0.07g:} \quad L_{u,\Delta} = 180 - \frac{w}{3} - L_i \\ &\text{PGA=0.4g:} \quad L_{u,\Delta} = 135 - \frac{w}{3} - L_i \end{aligned} \tag{8}$$

L_i is the minimum calculated value of the lattice shell span and its value is 30m. If span is less than 30m, it is calculated by L_i. The initial slope and shape coefficient of the curve are related to w and f/L. Roof weight correlation coefficient S_w, rise span ratio correlation coefficient μ_{fl} and shape factor n_s are calculated from equation (9) to equation (11) respectively.

$$S_w = 240 \cdot \frac{120}{w} \quad \left(60\,\mathrm{kg/m^2} \le w \le 240\,\mathrm{kg/m^2}\right) \tag{9}$$

$$\mu_{fl} = 0.075\frac{L}{f} + 0.675 \quad \left(\frac{1}{7} \le \frac{f}{L} \le \frac{1}{3}\right) \tag{10}$$

$$n_s = \left(1.02 - \frac{w}{7200}\right)\left(0.05\frac{L}{f} + 0.75\right) \tag{11}$$

Finally, by introducing the reduction factor r_b and the ground motion correction factor r_e, and adding the minimum stiffness ratio of 0.05 for safety consideration, the calculation formula of the limit stiffness ratio was obtained as follow:

$$\alpha_{k,min} = \frac{r_e}{r_b} \frac{L_\Delta}{S_w \mu_{fl}} \frac{1}{\left[1-\left(L_\Delta / L_{u,\Delta}\right)^{n_s}\right]^{1/n_s}} + 0.05 \tag{12}$$

The comparison between the limit stiffness obtained by formula (12) and the results numerical simulation (NS) is shown in Fig. 20 and Fig. 21. The theoretical calculation formula fits the limit stiffness ratio accurately. The limit stiffness ratio under PGA of o.4g is the recommended value for design, and the stiffness ratio in design should be greater than this value.

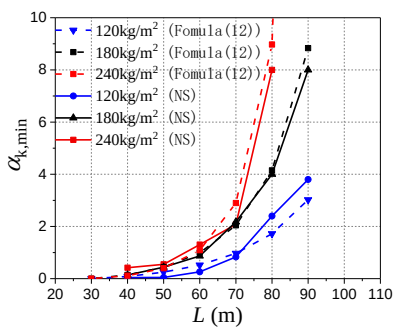

(a) Span-rise span ratio

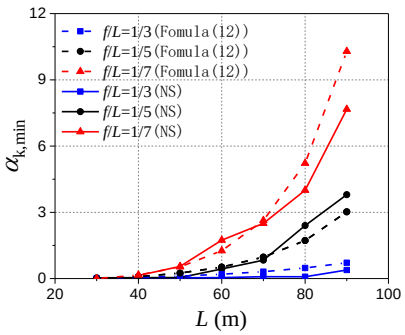

(b) Span - roof weight

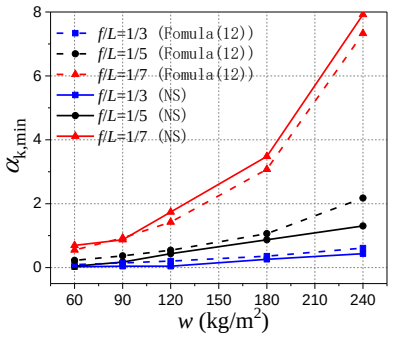

(c) Roof weight-rise span ratio

Fig. 20 Verification of limit stiffness ratio (PGA = 0.07g)

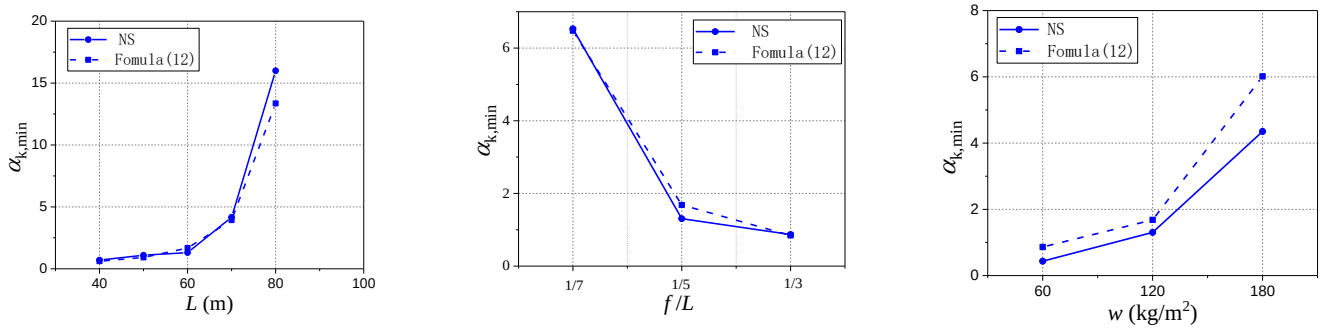

(a) Different span (b) Different rise span ratio (c) Different roof weight

Fig. 21 Verification of limit stiffness ratio (PGA = 0.4g)

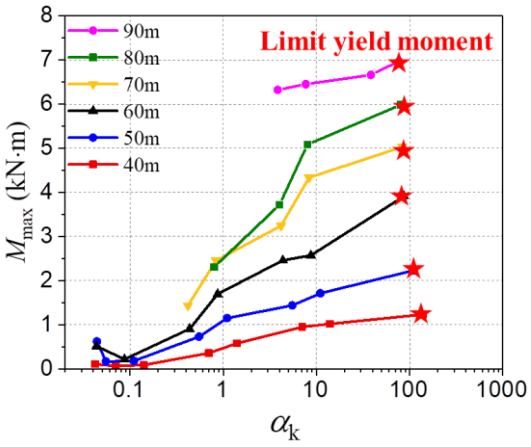

(a) Different span

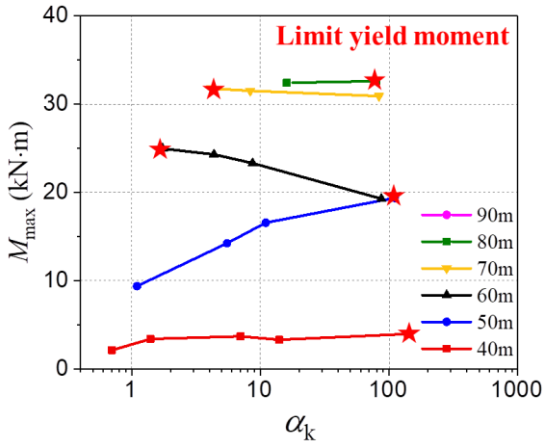

(a) Different span

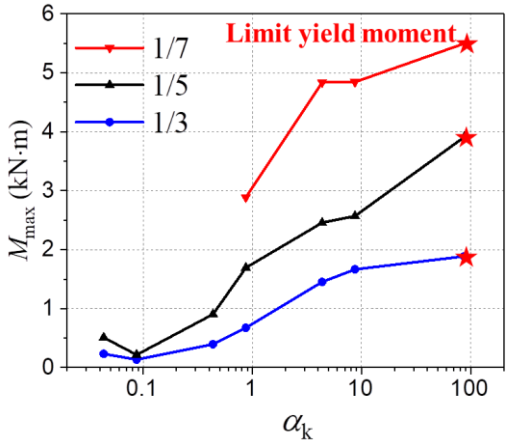

(b) Different rise span ratio

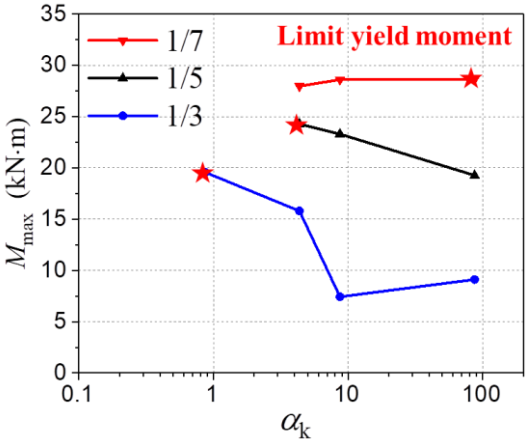

(b) Different rise span ratio

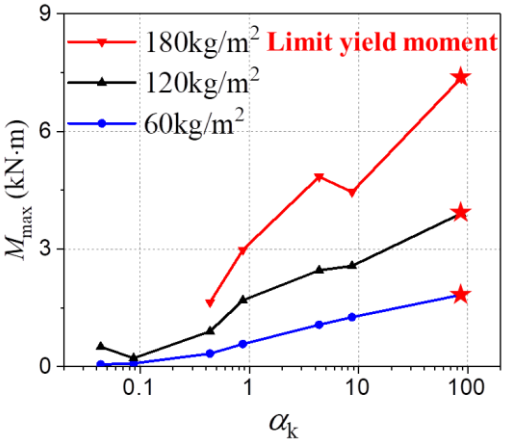

(c) Different roof weight

Fig. 22 Variation of M_{max} (PGA = 0.07g)

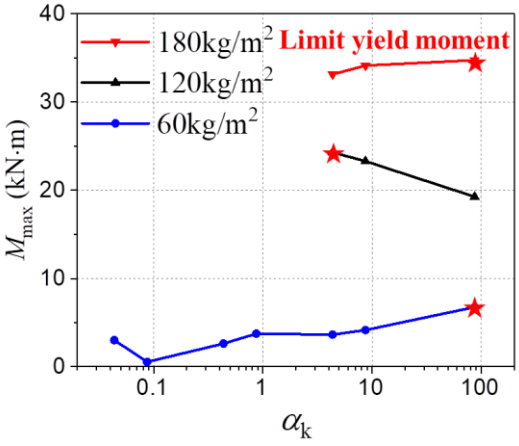

(c) Different roof weight

Fig. 23 Variation of M_{max} (PGA = 0.4g)

6. Analysis and calculation method of the limit yield moment of joint

After obtaining the joint stiffness used in the design, it is necessary to determine the design parameters of joint bending moment. Fig. 22 and Fig. 23 show the variation of the maximum bending moment response of the joints (M_{max}) in SRSS with different parameters and the stiffness ratio. As shown in the figures: i) with the increasing of span, roof weight and reduction of rise span ratio, the maximum moment response increases. ii) When the PGA is small (0.07g), the maximum moment response of the joints rises with the increase of joint stiffness. iii) However, in the condition of large PGA (0.4g), the local node displacement will be too large due to the yielding of members, which leads to the sudden increase of the moment response of nodes. The peak point of each curve is extracted, whose ordinate is recorded as the limit yield moment of joint (M_j). Taking this value as the seismic design parameter of the joint moment, the yield moment of joints used in the design should be greater than M_j.

The M_j of the SRSS with different parameters is drawn in Fig. 24, which shows that the limit yield moment of joint increases with the increasing of L, w and decline of f/L. And the larger the PGA is, the larger the limit yield moment is. The asterisk point in the figure is the example with span of 90m and PGA of 0.4g, in this condition, no matter how the stiffness and yield moment of joints are strengthened, the structure will still collapse. At this time, it needs to adopt other measures such as increasing the section of members and changing the rise span ratio of reticulated shell to keep the structure stable under earthquake action

According to the influence of L, f/L and w of the SRSS on M_{max}, M_j is obtained by formula (13) and formula (14) when the peak ground acceleration PGA = 0.07g and 0.4g respectively.

$$\text{PGA=0.07g:}\quad M_j=(0.15L-4.5)\left(0.2\frac{L}{f}\right)(0.01w-0.2) \tag{13}$$

PGA=0.4g:

$$M_j=\left[33-0.015(L-80)^2\right]\left(0.04\frac{L}{f}+0.8\right)(0.01w-0.2) \tag{14}$$

The good calculation accuracy of the theoretical formula is verified by comparing with the numerical simulation results, which can accurately fit the limit yield moment of joints in SRSS. The limit yield moment of the joint under the PGA of 0.4g is the recommended value in the design, and the joint yield moment in the design should be greater than this value.

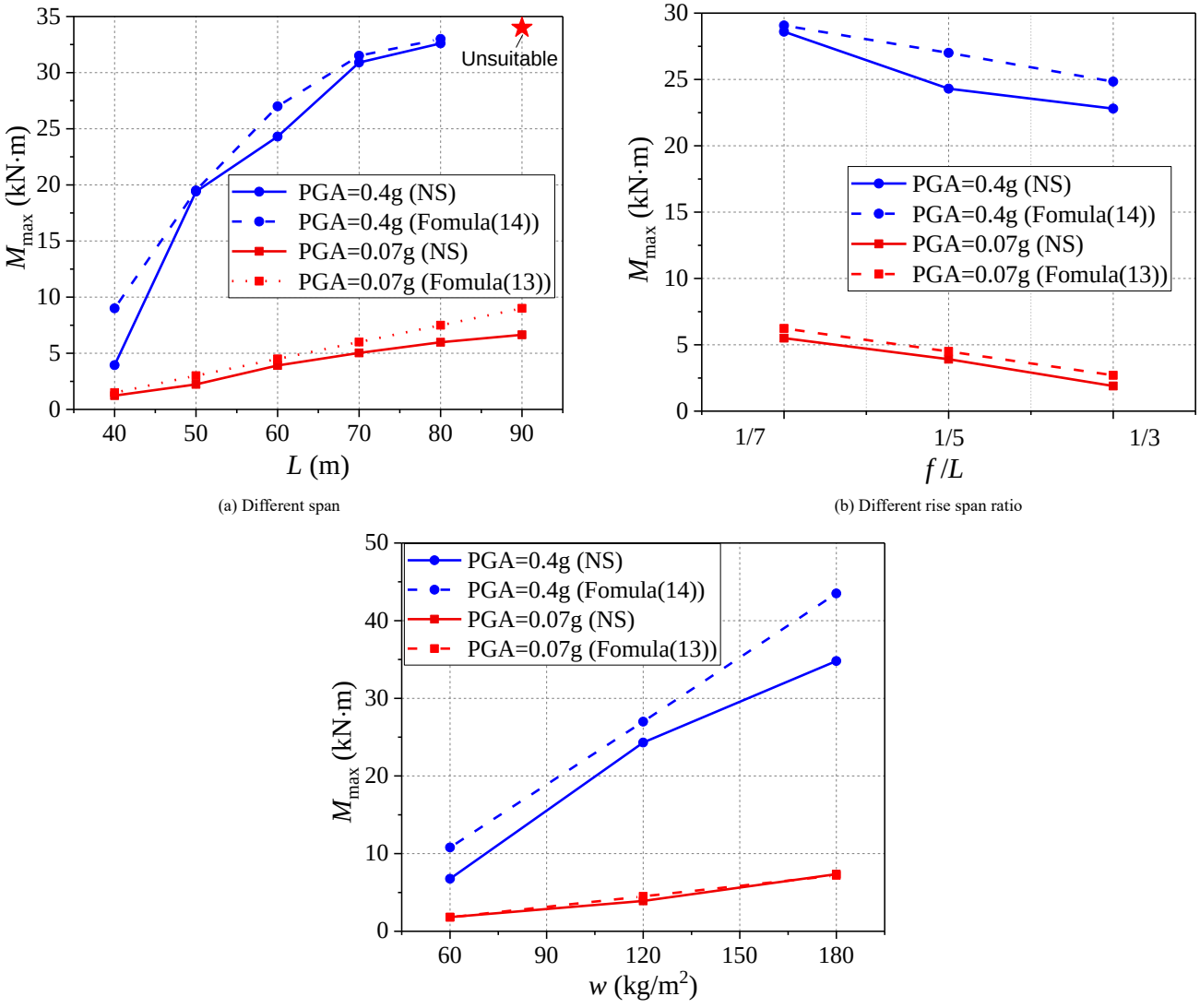

(a) Different span

(b) Different rise span ratio

(c) Different roof weight

Fig. 24 Verification of limit yield moment of joints

7. Conclusion

In this paper, the FEM of the semi-rigid reticulated shell was established to investigate the influence of joint stiffness on the seismic performance of semi-rigid SRSS. Large-scale parametric analysis was conducted. The following are the primary conclusions:

(1) The impact of stiffness ratio on the seismic performance of SRSS with semi-rigid joints was obtained, and two design parameters based on joint performance are proposed: the limit stiffness ratio and the limit yield moment.

(2) The effect of span, roof weight and rise span ratio on the limit stiffness ratio and limit yield moment were obtained. The fitting formulas for calculating the limit stiffness ratio and the limit yield moment of semi-rigid SRSS with different parameters were proposed.

(3) The seismic internal force coefficients of main member, circle member and diagonal member in semi-rigid SRSS were obtained, which can be used for seismic design of semi-rigid SRSS.

Acknowledgments

This research was supported by the National Science Fund for Distinguished Young Scholars (Grant No. 51525802), Shanghai Rising-Star Program (B type) Foundation (21QB1403100).

References

[1] Makowski Z S. Space structures of today and tomorrow[C]//Nooshin H.Third international conference on space structures. London.
[2] Richardson J N, Adriaenssens S, Coelho R F, Bouillard P. Coupled form-fnding and rigid optimization approach for single layer grid shells[J]. Engineering Structures, 2013, 52(9): 230–239.
[3] Fan F, Ma H H, Chen G B, et al. Experimental study of semi-rigid joint systems subjected to bending with and without axial force[J]. Journal of Constructional Steel Research, 2012, 68: 126–137.
[4] Ma H H, Fan F, Chen G B, et al. Numerical analyses of semi-rigid joints subjected to bending with and without axial force [J]. Journal of Constructional Steel Research, 2013, 90: 13-28.
[5] Ma H H, Wang W, Zhang Z H, et al. Research on the static and hysteretic behavior of a new semi-rigid joint (bcp joint) for single-layer reticulated structures[J]. J. IASS, 2017, 58(2): 159-172.
[6] Xue S D, Li S Y, Li X Y, Chen Y. Behaviour and mathematical model for semi-rigid threaded-sleeve connection[J]. Advanced Steel Construction, 2019, 15(2): 123–128.
[7] Jiang Y Q, Ma H H, Zhou G T, Fan F. Parametric and Comparison Study of a New and Traditional Aluminum Alloy Joint Systems[J]. Advanced Steel Construction, 2021, 17(1): 50-58.
[8] Ma H H, Ma Y Y, Yu Z W, et al. Experimental and numerical research on gear-bolt joint for free-form grid spatial structures[J]. Engineering Structures, 2017, 148: 522-540.
[9] Ma H H, Ren S, Fan F. Experimental and numerical research on a new semi-rigid joint for single-layer reticulated structures[J]. Engineering Structures, 2016, 126: 725–738.
[10] Mashrah W, Chen Z H, Liu H B, Amer M. Experimental, numerical, and theoretical study on static behaviour of novel steel dovetail joint subjected to axial tensile load [J]. Advanced Steel Construction, 2022, 18(1): 453-464.
[11] Ma R Q, Zhao P Y, Ban H Y, et al. Behaviour of reinforced joints between steel beam and L-shaped wide limb composite column[J]. Advanced Steel Construction, 2021, 17(1): 66–72.
[12] Ma H W, Zheng H, Zhang H, Tang Z Z. Experimental and numerical study of mechanical properties for the double-ribbed reinforced beam-column connection[J]. Advanced Steel Construction, 2020, 16(4): 297–309.
[13] Ma H H, Wang W, Zhang Z H, et al. Research on the static and hysteretic behavior of a new semi-rigid joint (bcp joint) for single-layer reticulated structures[J]. J. IASS, 2017, 58(2): 159-172.
[14] Ma Y , Ma H , Yu Z , et al. Experimental and numerical study on the cyclic performance of the gear-bolt semi-rigid joint under uniaxial bending for free-form lattice shells[J]. Journal of Constructional Steel Research, 2018, 149(OCT.):257-268.
[15] See T. Large displacement elastic buckling space structures[D]. Cambridge University, England, 1983.
[16] Fathelbab F A. The effect of joints on the stability of shallow single layer lattice domes[D]. University of Cambridge, England, 1987.
[17] El-sheikh A I. Effect of composite action on the behaviour of space structures[D]. University of Cambridge, England, 1992.
[18] Ma H H, Fan F, Zhong J, et al. Stability analysis of single-layer elliptical paraboloid latticed shells with semi-rigid joints[J]. Thin Walled Structures, 2013, 72: 128-138.
[19] Ma H H, Fan F, Wen P, et al. Experimental and numerical studies on a single-layer cylindrical reticulated shell with semi-rigid joints[J]. Thin Walled Structures. 2015, 86(1): 1-9.
[20] Gidófalvy K, Katula L, Ma H H. Free-form grid shell structures on rectangular plan with semi-rigid socket joints[J]. J. IASS, 2016, 55(4): 295-305.
[21] Ma H H, Issa A, Fan F, et al. Numerical study and design method of a single-layer spherical reticulated dome with hollow ball-tube bolted joints[J]. J. IASS, 2017, 58(2): 137-144.
[22] Jun Liao，Yigang Zhang，Jingzhi Wu. The dynamic elastic-plastic analysis of reticulated shell with semi-rigid connections [J]. Steel Construction, 2010, 25(9): 11-14.
[23] Feng Fan， Minling Wang， Zhenggang Cao. Seismic behavior and design of spherical reticulated shells with semi-rigid joint system [J]. China Civil Engineering Journal, 2010, 43(4): 8-15.
[24] Limin Li, Xingfei Yuan. Influence of joint stiffness on dynamic performance of the single-layer reticulated shell [J]. Spatial Structures, 2011, 17(3): 92-96.
[25] Xue S D, Wang N, Li X Y. Study on shell element modeling of single-layer cylindrical reticulated shell[J]. Journal of the International Association for Shell & Spatial Structures, 2013, 54(175): 57-66.